



Synthesis and characterization of ZnO NPs-doped PMMA-BDK-MR polymer-coated thin films with UV curing for optical data storage applications

A. A. Ahmad¹ · A. M. Alsaad¹ · Qais M. Al-Bataineh¹ · M-Ali H. Al-Akhras¹ · Zaid Albataineh² · Kholoud A. Alizzy¹ · Nermeen S. Daoud¹

Received: 26 May 2019 / Revised: 6 January 2020 / Accepted: 4 March 2020 / Published online: 9 March 2020
© Springer-Verlag GmbH Germany, part of Springer Nature 2020

Abstract

Hybrid material of poly-methyle-methacrylate (PMMA)-benzyl-dimethyl-ketal-azo dye methyl red (MR) thin film composites doped by various concentrations of ZnO NPs have been dip coated on glass substrates. The existence of azo dye (MR) in the composite was intentional to give the solution the desired pH level and to induce the *cis* ↔ *trans* cycles through illumination ↔ thermal relaxation. The optical and structural properties of the as-prepared thin films are investigated in relevance to ZnO NPs contents and the period of UV light illumination (short- and long-wavelength UV light). We found that the PMMA-BDK-MR doped by 1% ZnO NPs could be successfully used in optical data storage by implementing this composite in the WRITE/READ/ERASE cycle repeatedly. Specifically, it was found that the absorption band of the PMMA-BDK-MR doped by 1% ZnO NPs thin film lies between 350 and 600 nm upon illumination with 366 nm UV light for 10 s. Thermogravimetric analysis (TGA) was used to investigate the thermal stability of PMMA-BDK-MR/ZnO NPs. The TGA results are presented and interpreted. Furthermore, we investigated annealed poly-methyle-methacrylate-benzyl-dimethyl-ketal-methyl-red (PMMA-BDK-MR) doped by 1% ZnO NPs thin films. The *trans*–*cis* cycle has been repeated sequentially to confirm the hysteresis behavior for possible data READ/ WRITE or ERASE memory applications.

Keywords Thin Films · Hybrid materials · Optical data storage · ZnO nanoparticles (ZnO NPs) · Poly-methyle-methacrylate (PMMA) · Benzyl-dimethyl-ketal (BDK) · Azo dye methyl red (MR) · UV curing

✉ A. M. Alsaad
alsaad11@just.edu.jo; amalsaad@uno.edu

¹ Department of Physical Sciences, University of Science and Technology, P.O. Box 3030, Irbid 22110, Jordan

² Electronic Engineering Department, Yarmouk University, Irbid, Jordan

Introduction

Optical storage is the storage of data on an optically readable medium that has attracted much attention in the technology of optical reader heads. Optical storage provides superior memory capacity than magnetic storing because laser beams can be directed and focused more precisely than can magnetic heads do, thereby enabling the condensation of data into a much smaller space. Currently, the synthesis and design of new hybrid materials (Organic–Inorganic materials) have become one of the most interesting researches as they gain tremendous momentum by enabling the combination of the properties of inorganic elements and polymer matrices [1–5]. Organic materials possess several attractive properties such as easy processing with conventional techniques, elasticity, organic functionalities. Inorganic oxide materials have different properties such as hardness, thermal and chemical stability and transparency. Thus, hybrid materials combining the properties of organic polymers with properties of inorganic oxides are expected to possess very interesting physical and chemical properties. The properties of the hybrid materials can be varied and monitored continuously by controlling the organic/inorganic ratio and thus facilitate the “tailoring” of certain properties to form coatings for particular purposes [6]. Photocatalyst [7], hydrophilic [8, 9] or hydrophobic [10] coatings on heat-resistant substrate have already been prepared using simple fabrication techniques such as solgel [11].

Zinc oxide (ZnO) has attracted much attention due to its potential to be used as an additive in rubbers, plastics, ceramics, glass, cement, lubricants, paints, ointments, adhesives, sealants, pigments, batteries, ferrites, fire retardants and first aid tapes. These attributes make polymer/ZnO nanocomposites materials potentially interesting for several applications such as UV shielding, catalysis, field emission display, gas sensing, thermoelectricity, etc. [12]. Previously, ZnO nanoparticles were mixed with poly-methyle-methacrylate [13], polyimide [4, 14], poly(hydroxyl-ethyl-methacrylate) [15], poly(ethylene-glycol) [16], poly(ethylene-oxide) [17] and nylon-6 [18] to extremely improve their properties.

The materials containing [$>A=B<$] chromophore groups have gained considerable interest due to their potential applications in optical data storage devices, optical switching, optical limiting, signal processing, optical modulators, holography, nonlinear optical devices and photonic devices [19–29]. Azo dyes have been classified as good organic colorants consisting of at least a conjugated chromophore azo ($-N=N-$) group in association with one or more aromatic or heterocyclic systems. The spectral and photophysical properties of azobenzene are highly sensitive to their substitution pattern. A common feature to all azobenzene derivatives is the efficient and reversible photoisomerization between a thermally stable *trans*-state and a metastable *cis*-state upon absorption of a photon. *Trans*–*cis* isomerization process of polymers plays an important role in optical data storage applications [30–32].

Previous research works have used azobenzene carboxylic acid (azo dye) and methyl red (MR) as azobenzene-containing polymer films [33], azo dye-doped polymer waveguide [34], azo polymer material [35] and azo polymer waveguide

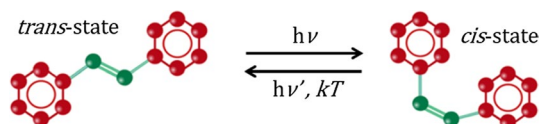
[36]. In this work, the switching process is controlled by azo hybrid material of poly-methyle-methacrylate-benzyl-dimethyl-ketal-methyl red (PMMA-BDK-MR) doped by inorganic ZnO nanoparticles.

We proposed a hybrid material of organic compound PMMA-BDK-MR doped by inorganic ZnO nanoparticles thin films for optical application such as light sensors or READ/WRITE/ERASE (WRE) optical data storage media for the UV light READ/WRITE heads. The composite is prepared by depositing PMMA-BDK-MR/ZnO NPs on glass substrate to obtain 500-nm film thickness by solgel dip coating technique. Up to the best of our knowledge, we are not aware of any experimental study that has previously investigated PMMA-BDK-MR/ZnO NPs for optical application such as light sensors or READ/WRITE/ERASE optical data storage media.

Trans–cis photoisomerization process

The principle mechanisms of photoexcited modulation of absorption in our composite may include photoinduced population changes, angular hole burning, molecular reorientation and *trans-cis* photoisomerization [37, 38]. We focus on the effect of ZnO NPs doped in azo dye PMMA-BDK-MR polymer for optical data storage applications. The azo dye polymers have attracted extensive attention due to their ability of converting their electrochemical state at room temperature from *trans* to *cis* configuration under photoisomerization process. They also can return to their *trans*-state under thermal relaxation process. This cyclic behavior made the azo dye composites potential candidates in WRITE/READ/ERASE (WRE) cycles for optical data storage devices or heat and light sensors [39–41]. Usually, at room temperature, the composite is initially in *trans*-state since the *trans*-isomer is thermally stable at room temperature. Upon illumination with UV light (or probably visible light), the composite undergoes electrochemical photoisomerization process (*cis*-state). In this conversion process, the electrochemical structure of the isomer goes through symmetric or antisymmetric twisting configuration of one aromatic bond without breaking it. In such case, the mono-molecule of the isomer extends or shrinks in its length which ultimately leads to a sequence change in the absorption band of the material [42, 43]. The change in the absorption band is linked with the change in material optical band gap energy. Figure 1 shows the *trans-cis* cyclic changes including the change in the mono-molecule bond length. The ring shown inside the cycle is a demonstration for one benzene ring. This new configuration is utilized as a state of memory WRITE or memory READ state. In addition, *cis*-state can be transferred back to *trans*-state by means of thermal relaxation process. This feature is used as an indicator for memory ERASE state. The cycles of *trans*↔*cis* flip-flop states can be achieved by repeating the illumination↔thermal relaxation processes for several times. Hence, the hysteresis process examines the reliability of using

Fig. 1 The complete photochemical mechanism involved in the real-time recording and erasing process [45]



the polymeric composites for memory READ, memory WRITE and memory ERASE states as seen in Fig. 1 [44]. Previous studies have shown that the PMMA thermal degradation process takes place. It is expected that the presence of ZnO NPs in PMMA-BDK-MR would shift the random scission process toward the higher temperature. Therefore, the presence of ZnO NPs improves thermal properties of PMMA-BDK-MR azopolymer that would influence its photonic and optoelectronic applications positively. The thermal stability of the cis-isomer depends on the influence of the substituent on the conjugated system. As the bonding degree between the substituent and the conjugated system is increased, the impact of the substituent increases, the thermal stability of the cis-isomer is reduced, and the rate of cis-to-trans isomerization accelerates. Substituents affect the resonance conjugation mode by affecting the π and π^* orbitals of the compounds. Thus, molecular orbital fluctuations can be adjusted so that the $\pi - \pi^*$ band of the compound can be shifted to separate $\pi - \pi^*$ transition bands of the cis–trans isomers. This allows cis–trans isomerization in the visible region, which has a very important significance in terms of practical photonic and optoelectronic applications. Introducing ZnO NPs in the PMMA-BDK-MR results in a large $\pi - \pi^*$ band separation in the cis- and trans-isomers. It also shows the fast cis–trans isomerization rate. The cis-isomer shows a good thermal stability, with a half-life of up to 4795 h at room temperature.

Experimental details

In this section, the materials, the synthesis procedure of organic composite PMMA-BDK-MR/ZnO NPs with different concentrations of ZnO nanoparticles and characterizations methods are described in details.

Materials

Poly-methyle-methacrylate (PMMA)

Poly-methyle-methacrylate (PMMA) is a transparent thermoplastic produced from the polymerization of methyl methacrylate. PMMA is an ester of methacrylic acid ($\text{CH}_2=\text{C}[\text{CH}_3]\text{CO}_2\text{H}$) that belongs to the important acrylic family of resins [45].

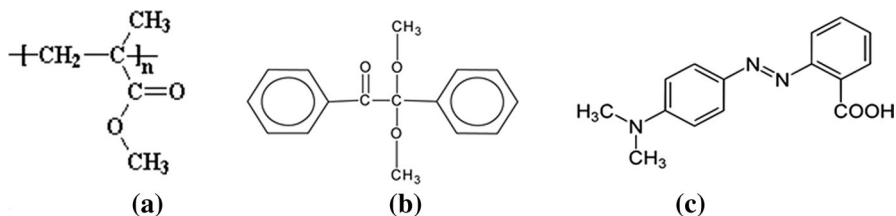


Fig. 2 The structures of: **a** PMMA, **b** BDK and **c** MR compounds

The structure of PMMA is shown in Fig. 2a. Poly-methyle-methacrylate powder with a molecular weight of 120,000 g/mol was purchased from Sigma-Aldrich.

Benzyl-dimethyl-ketal (BDK)

Benzyl-dimethyl-ketal (BDK) is a free radical photoinitiator designed for UV-curable applications through seeding free radical in composite [46]. The molecular formula of BDK is $[C_{16}H_{16}O_3]$. Polymerization started by photoinitiators leads to the high light sensitivity of BDK. BDK is insensitive to temperature changes and easy to be controlled [47, 48]. Upon photoinitiation, the BDK undergoes a fragmentation of its structure upon exposure to ultraviolet radiation initiating the polymerization process [49]. The structure of BDK is shown in Fig. 2b. Benzyl-dimethyl-ketal (BDK) powder of molecular weight of 254.30 g/mol was purchased from Sigma-Aldrich.

Azo dye methyl red (MR)

The molecular formula of azo compounds have the form of $R-N=N-R_1$, in which R and R_1 can be either aromatic or aliphatic [50]. The aromatic azo compounds are usually stable and have different colors, such as red, orange or yellow. Therefore, they are used as dyes. The chemical formula of the MR is $C_{15}H_{15}N_3O_3$. MR can be used as acid–base indicators due to their ability to function as weak acids [44]. The structure of MR is shown in Fig. 2c. Methyl red powder was purchased from SCP.

Treatment of the substrates

The glass substrates were pre-cleaned to remove the surface oxidized layer and greases. They were cleaned with warm tap water then rinsed with ionized acidic water of $pH = 3.5$ and finally dipped in acetone. The substrates were then bathed in ultrasonic path of distilled water for five minutes and dried with cold air.

Preparation ZnO nanoparticles by hydrothermal technique

ZnO nanoparticles of 50 nm in diameter were prepared by dissolving 1.2 g of zinc acetate dehydrates $Zn(CH_3CO_2)_2 \cdot 2H_2O$ in 20 ml of ethanol under magnetic stirring. A volume of 0.3 g NaOH dissolved in 20 ml ethanol was added to the solution drop by drop under stirring for 30 min. The solution was then carried into water bath maintained at a temperature of 70 °C for 3 h. The obtained ZnO nanoparticles (ZnO NPs) were washed by ethanol and distilled water in order to remove impurities and finally dried in air at 50 °C for 24 h [51, 52].

Preparation of PMMA-BDK-MR/ZnO NPs films

PMMA-BDK-MR organic composites in the form of solution were prepared. We used 0.3 g of PMMA, 0.3 g of photoinitiator (BDK) and a 0.3 g of azo dye (MR) of pH (4.2–4.6), each dissolved separately in 30 ml tetrahydrofuran. The mixed

solution with the volume fractions was then filtered using 0.45- μm Millipore filter before dip coating on the glass substrates. All films were prepared at standard conditions (i.e., room temperature of 25 °C and 1 atmospheric pressure). The mixture blend was made of the following volume fractions (3 of PMMA, 3 of BDK, 1 of MR). Hybrid material of PMMA-BDK-MR organic composites doped by inorganic ZnO nanoparticles concentrations of 1, 2 and 4% were prepared. Calculated amount of ZnO NPs was added directly into a flask to produce ZnO networking into PMMA-BDK-MR matrix. The solutions were finally stirred for 1 h, and each solution was then poured into a separate petri dish.

Dip coating and curing methods

Smooth films were obtained by dipping the glass substrate in the solution for one and half hour to get a film of 500 nm thickness. The films were dried and left to dry in air for twenty-four hours at least to evaporate the solvent and organic residues. Each sample was illuminated by either UV lamp (355 nm) or UV lamp (263 nm) with a power of 6 Watt for several periods. The absorbance of PMMA-BDK-MR/ZnO NPs thin films with different concentrations of ZnO NPs for different periods of light curing (0–240 s in steps of 5 s) was measured and recorded (not shown in the manuscript but available on request). We found that the best source of UV curing is the one with wavelength of 366 nm. The best curing time was found to be 10 s. The UV light was used instead of blue light because of the high absorption of the UV light by all components in the thin films (ZnO, BDK and MR), while blue light absorbed by MR component only. Furthermore, in the short exposure time, low-intensity UV light does not change the color of MR film. On the other hand, it is well known that azo dye undergoes a *trans*–*cis* transformation by a UV light activated photoisomerization process that usually takes only few seconds. However, a *cis* form could be transversed back to a *trans* form by means of thermal relaxation process. This thermally activated reversed *cis*–*trans* conversion process typically takes about an hour. Consequently, it does not contribute to any permanent change in the optical constants, while BDK activated by a transition within the molecular orbits of the $>\text{C}=\text{O}$ group followed by an α -splitting to produce free radicals when it irradiated by UV light [46].

Characterization of PMMA-BDK-MR/ZnO NPs thin films

A double beam UV–Vis spectrophotometer (U-3900H series) was used to measure the transmittance and reflectance spectra in the UV–visible range (250–700 nm). The transmittance and reflectance have been used to determine absorption coefficient (α), optical band gap energy (E_g), Urbach energy (E_U), optical constants (n and k), dielectric functions (ϵ_1 and ϵ_2) and dielectric loss tangent ($\tan \delta$). We investigated the potential of PMMA-BDK-MR/ZnO NPs thin films as READ/WRITE/ERASE (WRE) configurations and optical and heat sensors. EDAX mapping and SEM studies were performed to get a deeper insight into the structural properties and the surface morphology of PMMA-BDK-MR/ZnO NPs thin films.

Thermogravimetric analysis (TGA) of PMMA-BDK-MR/ZnO NPs thin films

We have used a simple setup built at our laboratory to investigate thermal stability of PMMA-BDK-MR/ZnO NPs thin films. It consists of a digital balance connected to coils, thermocouple and a power supply to obtain the TGA profiles of the investigated PMMA-BDK-MR/ZnO NPs polymeric thin films.

Results and discussion

WRE optical data storage cycle using PMMA/BDK/MR/ZnO NPs thin films

The optical characteristics of the PMMA/BDK/MR/ZnO NPs thin films with various ZnO NPs concentrations have been investigated by measuring the transmittance and the reflectance in the spectral range of 250–700 nm. The main objective of this part of our study is to investigate the effect of ZnO NPs content on the optical and structural properties of PMMA/BDK/MR thin films. Specifically, we investigate the curing time and the light source of curing (high energy UV 263 nm versus low energy UV 355 nm) required to obtain optimum absorbance of as-prepared PMMA/BDK/MR/ZnO NPs thin films. In searching for the most appropriate conditions, we found that 366 nm UV source for 10 s to be the best curing UV source and curing time for the best polarization process of PMMA-BDK-MR/ZnO NPs thin films as demonstrated in Fig. 3. It shows the absorbance spectra of PMMA-BDK-MR/ZnO NPs thin films exposed to UV curing. We noticed that the absorbance spectra have peaks in the spectrum region of (350–600) nm that contain green, blue and violet colors. This behavior is attributed to the existence of MR in the thin films that gives the films the reddish color. It is known that this red-colored thin film transmits red, yellow and orange lights, while it blocks other colors such as green, blue and violet. We

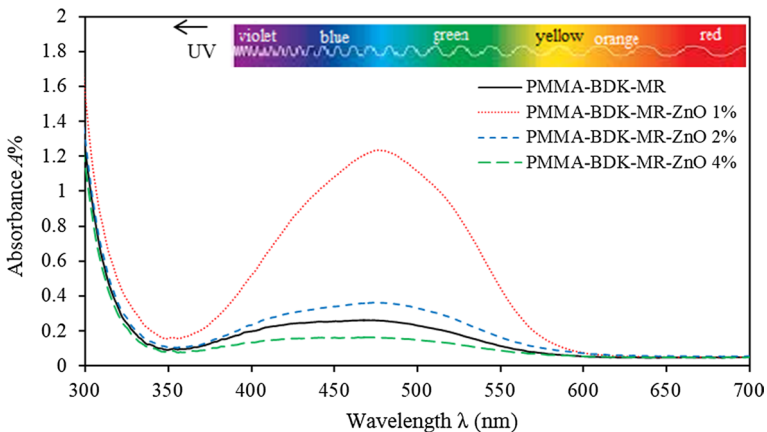


Fig. 3 Absorbance spectra of PMMA-BDK-MR/ZnO NPs thin films with various ZnO NPs concentrations treated with UV-366 nm curing for 10 s

found that the maximum absorption bands of PMMA-BDK-MR/ZnO NPs with ZnO NPs concentrations of 0%, 1%, 2% and 4% appear at 466, 476, 473.5 and 469 nm, respectively. These bands belong to the $\pi - \pi^*$ transitions of azo. The redshift of the absorption peaks upon introducing ZnO NPs into the polymer is due the strong electron withdrawing effect of ZnO NPs made the two electrons on the Zn of the ZnO molecule transfer to the nitrobenzene via azo double bond conjugated system [53]. The PMMA-BDK-MR/ZnO NPs 1% thin films have optimum values of absorbance in the region of (350–600) nm indicating that this thin film is highly polymerized.

Careful examination of Fig. 3 shows that the absorbance of PMMA-BDK-MR doped by 1% ZnO NPs thin film exhibits the highest peak in the spectral range of 350–600 nm. Consequently, this film would be excellent for optical data storage. This result is attributed to the fact that ZnO NPs have high transmittance and low absorbance in the visible region [51, 54]. Hence, introducing high concentrations of ZnO NPs in PMMA-BDK-MR matrix is expected to lead to a composite exhibiting low absorbance in the region between 350 and 600 nm. On the other hand, introducing low concentration of ZnO NPs (1%) in PMMA-BDK-MR yields composites with primarily high absorption peak at around 490 nm. The as-deposited films at room temperature are expected to be in *trans*-state before illumination and then traversed back to *cis*-state by illumination as illustrated in Fig. 1.

The PMMA-BDK-MR/ZnO NPs 1% thin films have been treated with optimized conditions of illumination. The as-prepared thin film then treated with thermal relaxation process under atmospheric conditions for one hour at 90 °C temperature. Figure 4 shows the absorbance of PMMA-BDK-MR/ZnO NPs 1% thin films without light curing and heat treatment. As expected, the thin films exhibit *trans*-state (black solid line, initial *trans*-state). The thin films are then illuminated by high UV light of wavelength of 366 nm for 10 s. As can be seen from Fig. 4, the films acquire different absorbance band (350–600 nm) at the middle of the visible range with a blueshift in the head of the peak transferring the material from

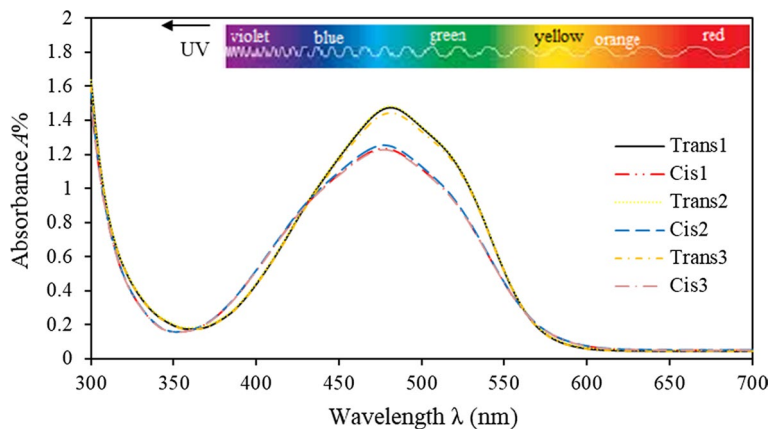


Fig. 4 Absorbance spectra of PMMA-BDK-MR/ZnO NPs/ZnO NPs 1% thin films, at Natural case, cis case after 10 s of UV-366 nm curing and trans after annealing at 90 °C

trans-state to *cis*-state as expected (Fig. 4, red dot-line, *cis*-state). This absorbance band in this range of the visible spectrum is expected because of the presence of MR in the PMMA-BDK/ZnO NPs 1% thin films. Finally, the films are thermally annealed for one hour at 90 °C. This process transfers thin films back to *trans*-state as proposed in Fig. 1. The transmittance of thin films before and after illumination and the heat processes are recorded and investigated for *trans*↔*cis* cyclic periodic behavior. Over the whole range of interest, the transmittance of the thermally treated thin films have been restored exactly as the transmittance before illumination (Fig. 4, yellow dashed line, *trans*-state again). In this case, we may consider writing a data unit by transferring the storage unit made of this material from *cis* to *trans* or *trans* to *cis*, just like switching “on” and “off” states in electrical circuits or “logic 1” and “logic 0” in the low-level language of the computer data storage media. This process has been repeated three times, and the cycle of *cis*↔*trans* has repeated itself exactly indicating a reliable hysteresis loop of “on” and “off” states, as shown in Fig. 5. The figure illustrates the maximum values of absorbance in the peak region in *trans* and *cis* forms. Odd numbers represent *trans* form and even numbers represent *cis* form. The absorption band is attributed to the $\pi - \pi^*$ transitions in twisting the MR azo dye monomolecular nanostructure as proposed in Fig. 1. The absorbance band in the visible region is attributable to the $S_0 - S_1$ transitions in the *cis* form that falls throughout the $S_0 - S_2$ transition of the *trans* form. The prolonged illumination does not change the shape of absorption spectrum, indicating that a photostationary state exists between *trans* and *cis* forms [39, 41].

Optical properties of all investigated thin films after curing

Optical properties can be obtained and interpreted in the view of the interaction between the incident photons and the as-prepared thin films. Figure 6 shows the transmittance spectra of PMMA-BDK-MR/ZnO NPs thin films for various ZnO NPs concentrations. The spectra are divided into three major regions: (a) the transparent

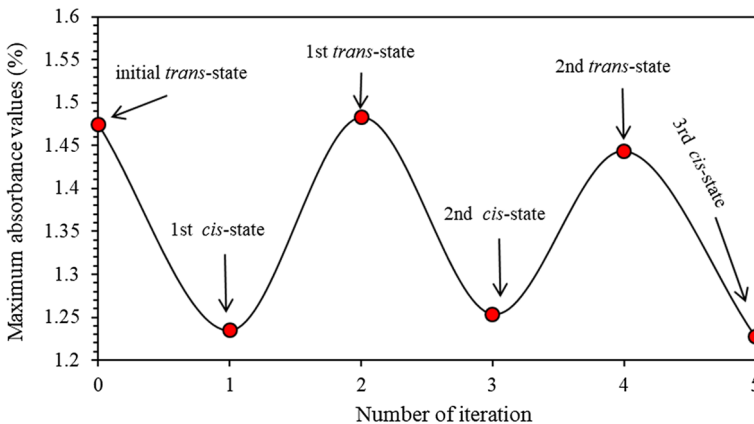


Fig. 5 Maximum absorbance value vs. number of iterations of transformation from *trans* to *cis*: odd numbers represent *trans* case and even numbers represent *cis* case

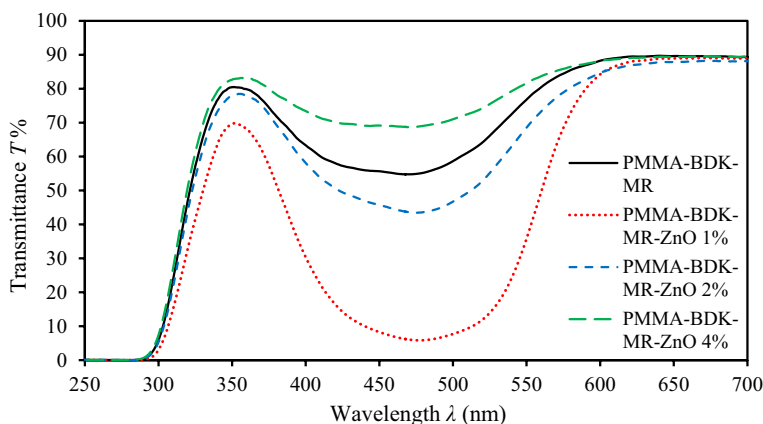


Fig. 6 Transmittance spectra of PMMA-BDK-MR/ZnO NPs thin films with various ZnO NPs concentrations treated by UV-366 nm curing for 10 s

region in the wavelength range $\lambda \geq 600$ nm, (b) the region with low transmittance (high absorbance in the wavelength range $350 < \lambda < 600$ nm and (c) the high absorption region occurs in the wavelength range $\lambda \leq 350$ nm. The spectral range (350–600) nm contains green, blue and violet colors is the range of absorbance due to the existence of MR in the samples that gives the films the reddish color which is in good agreement with the results obtained by Wang et al., Wu et al., and Ahmad and Omari [44, 55, 56]. It is obvious from Fig. 6 that PMMA-BDK-MR/ZnO NPs 1% thin films have minimum values of transmittance in the spectral region (350–600) nm. The reflectance of thin films was measured by the spectrophotometer implementing the total internal reflectance integrated sphere set in the reflectance mode. Similar argument applies to the reflectance spectra with opposite curve trends as shown in Fig. 7. The most interesting region in the reflectance spectra is the lowest wavelength region. A closer look at the inclination slope of the linear reflectance part indicates the absorbance tail trend, which leads to Urbach tail energy as will be discussed later.

For our hybrid material thin films, the study of the spectral behavior of the absorption coefficient gives significant information about the atomic vibrations in the lower energy part of the optical absorption spectrum and the electronic states in the high energy part of the spectrum [57, 58]. Absorption coefficient defined by $\alpha = 1/d \ln(1/T)$ where d is the thickness of the film measured by SEM micrograph and found to be 500 nm and T is the transmittance. Optical absorption spectra of PMMA-BDK-MR/ZnO NPs thin films for various ZnO NPs concentrations have been studied to determine the absorption coefficient (α), optical band gap (E_g), Urbach energy (E_U) and the nature of the electron transitions involved at the atomic scale. Figure 8 shows the absorption coefficient spectra of PMMA-BDK-MR/ZnO NPs 1%, 2% and 4% thin films. Figure 8 indicates that the absorption edge is located in the visible region. Furthermore, the position of absorption edge depends on composition of thin films as illustrated in Fig. 9. Using Fig. 9, we calculate the optical band gap values of the thin films. We found that undoped PMMA-BDK-MR thin

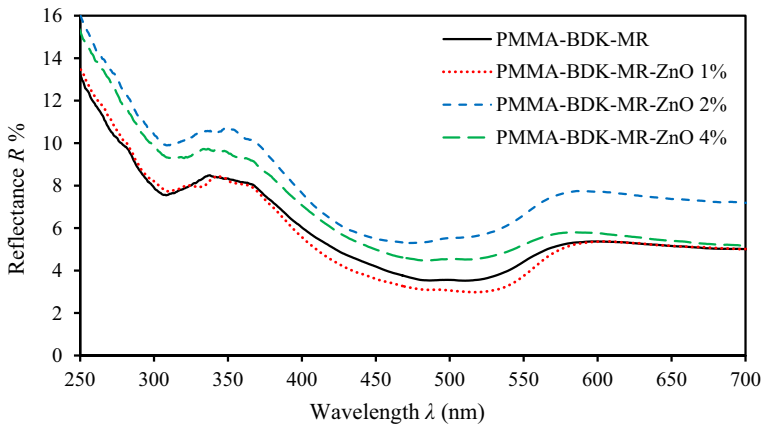


Fig. 7 Reflectance spectra of PMMA-BDK-MR/ZnO NPs thin films with various ZnO NPs concentrations treated by UV-366 nm curing for 10 s

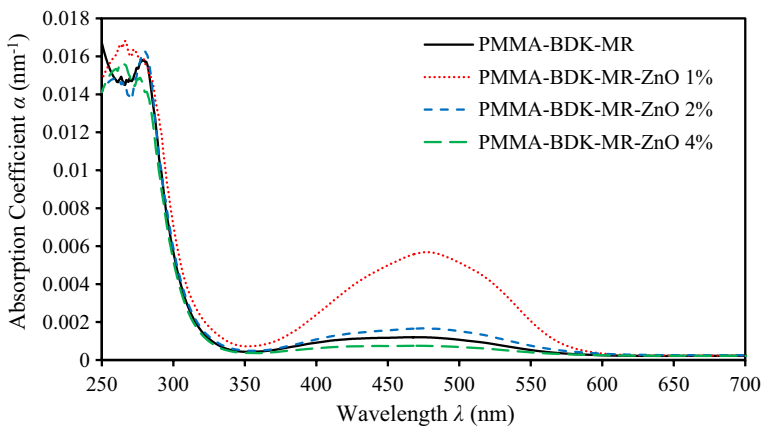


Fig. 8 Absorption coefficient spectra of PMMA-BDK-MR/ZnO NPs thin films with various ZnO NPs concentrations treated by UV-366 nm curing for 10 s

film exhibits an optical band gap of 3.920 eV. Upon incorporating 1%, 2%, and 4% of ZnO NPs into PMMA-BDK-MR thin film, optical band gap has decreased to 3.858 eV, 3.895 eV and 3.905 eV, respectively. Thus, our results obviously indicate that it is possible to engineer the optical band gap of the as-prepared polymeric thin films by merely controlling the concentration of ZnO NPs.

The absorption coefficient (α) is related to photon energy ($h\nu$) by $(\alpha h\nu)^{1/n} = \beta(h\nu - E_g)$ [59]. Here, β is a constant called band tailing parameter, E_g is the optical band gap energy, n is the power factor of the transition mode that depends on the nature of the material. To examine whether the optical band transition mode is direct or indirect, the above equation is rearranged to become

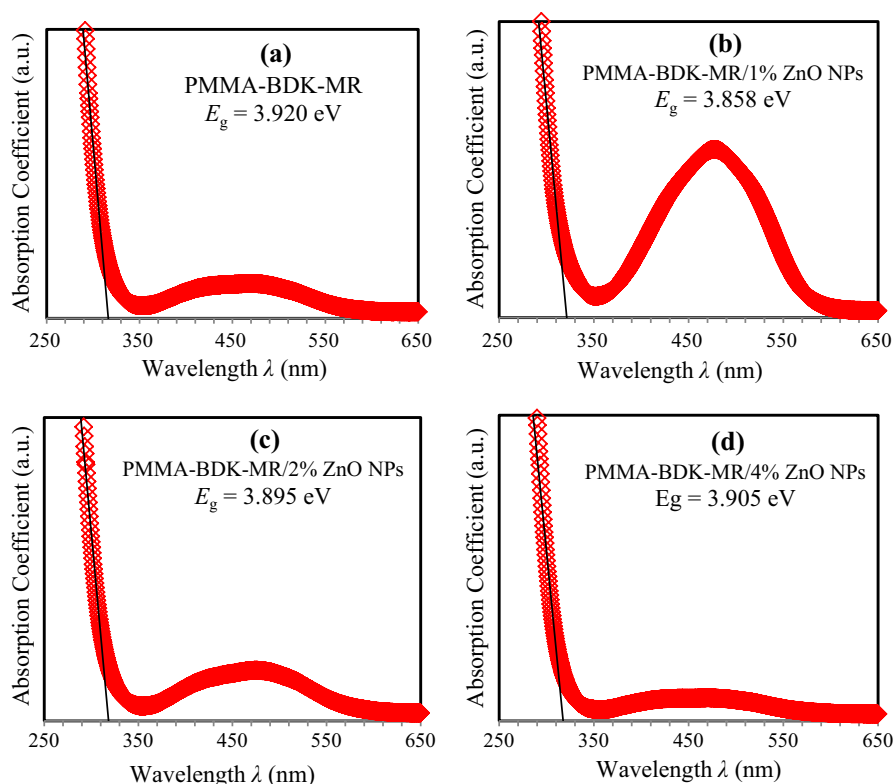


Fig. 9 The shift of absorption edge and optical band gap energy values of PMMA-BDK-MR/ZnO NPs thin films with various ZnO NPs concentrations at treated by UV-366 nm curing for 10 s: **a** PMMA-BDK-MR **b** PMMA-BDK-MR/ZnO NPs 1% **c** PMMA-BDK-MR/ZnO NPs 2% and **d** PMMA-BDK-MR ZnO NPs 4%

$\ln(\alpha h\nu) = \ln \beta + n \ln(h\nu - E_g)$ [60]. The value of power factor (n) identifies the type of the optical transition mode is basically the slope of the resultant straight line resulted from plotting $\ln(\alpha h\nu)$ on y -axis against $\ln(h\nu - E_g)$ on x -axis [60, 61]. We found the transition power factor (n) of all hybrid PMMA-BDK-MR/ZnO NPs thin films to be $3/2$ indicating that the films exhibit direct forbidden transitions. One may recognize some features of absorbance defined by an exponential relation at the lower part of the absorption coefficient spectra below the band edge. These extension features are called exponential tails known as Urbach tails. These tails appear in the poor crystalline, disordered and amorphous materials due to the localized states that extended into the band gap [35–37]. The mathematical modeling of the exponential tail known as Urbach empirical rule is given by: $\alpha = \alpha_0 \exp(h\nu/E_U)$, where α_0 is a constant, $h\nu$ is the incident photon energy and E_U is the band tail width (Urbach binding energy) of the localized states extended into the optical energy gap. The values of band tail width (Urbach binding energy = E_U) are shown in Table 1 for the PMMA-BDK-MR/ZnO NPs 1%, 2% and 4% thin films. According to this model,

Table 1 Optical band gap energy, Urbach energy, steepness parameter and electron–phonon interaction of PMMA-BDK-MR/ZnO NPs thin films with different concentrations of ZnO NPs

Sample	E_g (eV)	E_U (eV)	Steepness factor (σ) in eV	Electron–phonon interaction E_{e-p} (eV)
PMMA-BDK-MR/ZnO 0%	3.920	0.161	0.160	4.169
PMMA-BDK-MR/ZnO 1%	3.858	0.279	0.092	7.226
PMMA-BDK-MR/ZnO 2%	3.895	0.251	0.102	6.514
PMMA-BDK-MR/ZnO 4%	3.905	0.266	0.0965	6.902

E_U is evaluated as the reciprocal of the slope of the relationship of the incident photon energy ($h\nu$) versus ($\ln \alpha$). Moreover, Urbach suggested another formula to extract the absorption coefficient (α) and the optical band gap energy as $\alpha = \beta \exp \left[\frac{\sigma(h\nu - E_0)}{k_B T} \right]$ [38], where β is a pre-experimental constant and σ is the steepness parameter, E_0 is the transition energy equals to E_g for direct transitions and $E_g \pm E_p$ for an indirect transition. The parameter E_p is the phonon energy associated with the transition. Rearranging the equation, the steepness parameter is given by the relation: $\frac{(h\nu)}{E_U} = \frac{\sigma(h\nu)}{k_B T}$. The estimated values of the steepness factor (σ) are listed in Table 1. The steepness parameter (σ) is related also to the strength of the electron–phonon interaction (E_{e-p}) by $E_{e-p} = \frac{2}{3\sigma}$ [39]. Hence, the values of the strength of the electron–phonon interaction (E_{e-p}) can be estimated as reported by Table 1.

Complex refractive index \tilde{n} is a material property distinguishes a material from another by how it interacts with incident light photons. It governs the light–material interaction in terms of the change in light polarization (perpendicular and parallel amplitudes as well as the change in phase polarization), the speed of light inside the material and light intensities. Therefore, determining the index of refraction (ordinary and extraordinary components, if available) is of great interest to engineer the appropriate thin film materials for particular optical applications such as optical devices, switches, filters, photovoltaic, etc. [62]. Complex refractive index \tilde{n} is given by $\tilde{n} = n + ik$, where k is the extinction coefficient and n is the index of refraction. The extinction coefficient (k) is related to the wavelength by $k = \alpha\lambda/4\pi$. As depicted in Fig. 10, the extinction coefficient (k) of thin films over the range 350–600 nm observed to increase in a hub-like behavior due to the presence of MR and ZnO NPs treated with the proper light curing for optimum polarization. We found that PMMA-BDK-MR/ZnO 1% exhibits the highest value of k in the spectral range of 350–600 nm. The sharp decrease of k below 325 nm indicates the presence of major light absorption by thin films below 325 nm. It also indicates the presence of electrons transition from the valance band to the conduction band. The index of refraction (n) of thin films has been calculated using the equation $n = ((1 + R)/(1 - R)) + \sqrt{(4R/(1 - R)^2) - k^2}$. The resultant index of refraction as a function of incident light wavelength is shown in Fig. 11. The index of refraction

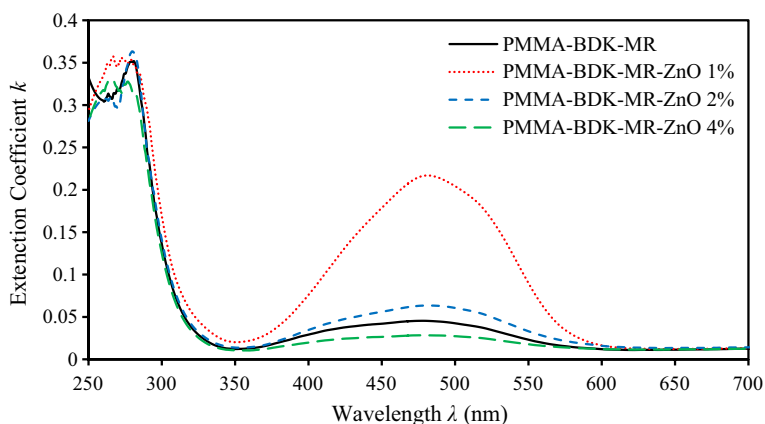


Fig. 10 Extinction coefficient spectra of PMMA-BDK-MR/ZnO NPs thin films with various ZnO NPs concentrations treated by UV-366 nm curing for 10 s

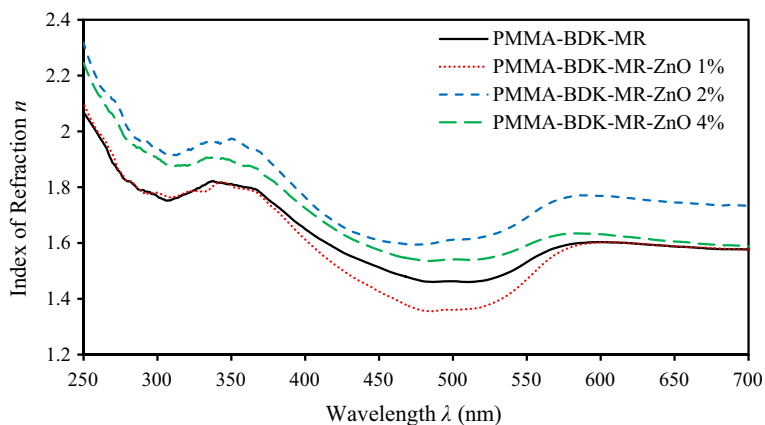


Fig. 11 Index of refraction spectra of PMMA-BDK-MR/ZnO NPs thin films with various ZnO NPs concentrations treated by UV-366 nm curing for 10 s

of undoped PMMA-BDK-MR exhibits values between 1.5 and 1.7 in the visible region.

The calculation of dielectric function is performed in terms of optical constants n and k related to ϵ_1 and ϵ_2 by $\epsilon_1 = n^2 + k^2$ and $\epsilon_2 = 2nk$ [63]. Figures 12 and 13 show the values of dielectric functions (ϵ_1 and ϵ_2) of PMMA-BDK-MR/ZnO NPs 1%, 2% and 4% thin films. Similar argument applied to n and k applies to parameters ϵ_1 and ϵ_2 . Dielectric loss factor ($\tan \delta$) is the ratio of the imaginary part of the dielectric constant of the real part. The dielectric loss is given by

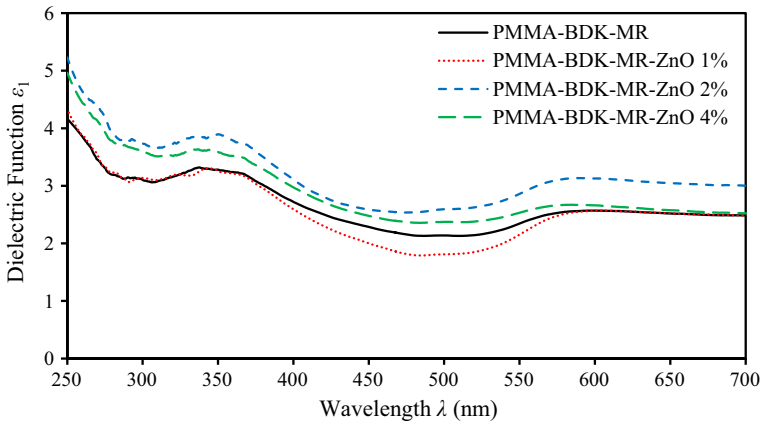


Fig. 12 Dielectric function ϵ_1 of PMMA-BDK-MR/ZnO NPs thin films with various ZnO NPs concentration treated by UV-366 nm curing for 10 s

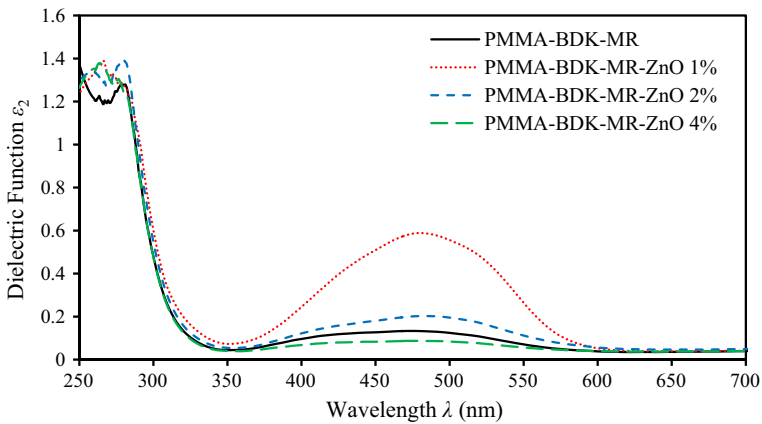


Fig. 13 Dielectric function ϵ_2 for PMMA-BDK-MR/ZnO NPs thin films with various ZnO NPs concentrations treated by UV-366 nm curing for 10 s

$\tan \delta = \epsilon_2 / \epsilon_1$ [64, 65]. Figure 14 shows the dielectric loss of PMMA-BDK-MR/ZnO NPs 1%, 2% and 4% thin films.

SEM micrograph, EDAX and mapping

Investigating the microstructure and the surface morphology of thin films is an important tool to understand their nature and functioning. The SEM micrographs technique was used to study the surface morphology of the PMMA-BDK-MR/ZnO NPs composite thin films. The study includes the individual reference PMMA-BDK-MR thin films; the PMMA-BDK-MR/ZnO NPs 1% thin films selected for

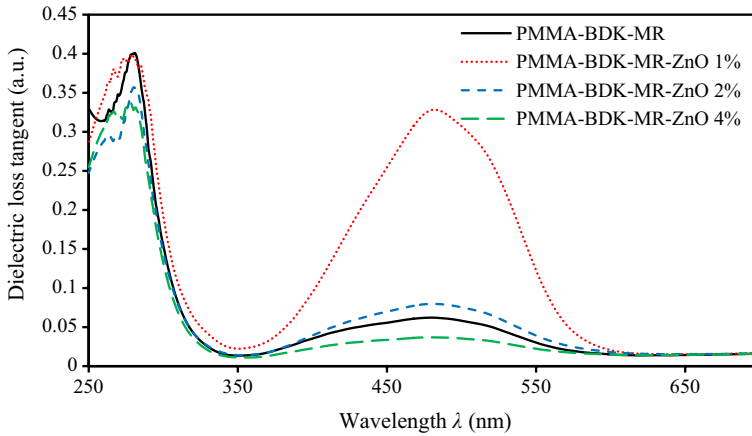


Fig. 14 Dielectric loss tangent ($\tan \delta$) for PMMA-BDK-MR/ZnO NPs thin films with various ZnO NPs concentrations treated by UV-366 nm curing for 10 s

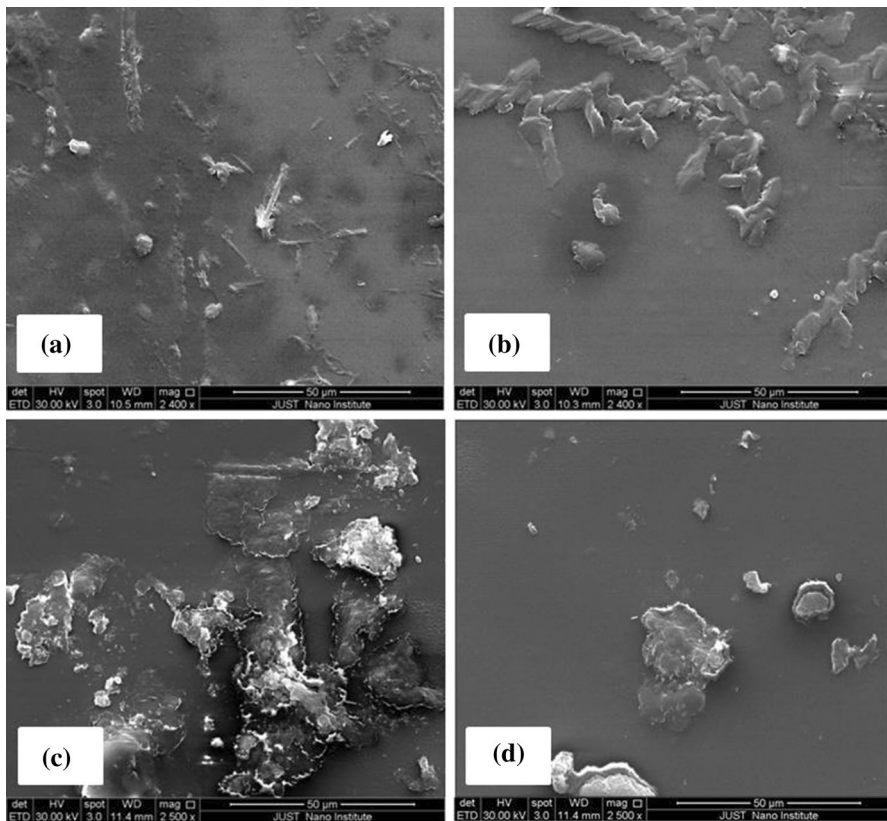


Fig. 15 SEM micrograph of **a** PMMA-BDK-MR without curing, **b** PMMA-BDK-MR with curing, **c** PMMA-BDK-MR/ZnO NPs 1% without curing, and **(a)** PMMA-BDK-MR ZnO NPs 1% with curing

optical data storage applications. A comparison study between the references morphologies and those of PMMA-BDK-MR/ZnO NPs 1% thin film deposited by dip coating technique are reported and interpreted. Figure 15 shows SEM micrograph of PMMA-BDK-MR and PMMA-BDK-MR/ZnO NPs 1% surface morphology before and after curing. We found that both have amorphous nature. Figure 15a–c depicts the SEM micrograph of PMMA-BDK-MR and PMMA-BDK-MR/ZnO NPs 1% without UV curing. Thin films without UV curing are found to have inhomogeneous surfaces compared with their surfaces after curing as can be clearly seen in Fig. 15b–d. The transformation from inhomogeneous surfaces to homogeneous surfaces is attributed to high degree of polymerization of the thin film by UV curing. The presence of as-deposited BDK material throughout the PMMA-host material takes random configuration. As the film is exposed to the UV light, the BDK is activated forming radical roots throughout the PMMA matrix causing content atoms to vibrate seeking the minimum potential energy positions. This reform process makes the surface morphology changes due to the UV exposure.

Figures 16, 17, 18 and 19 show qualitative analysis of the energy dispersive X-ray spectroscopy (EDAX) micrographs. The EDAX micrographs show the elemental constituent of thin films including the elements of the glass substrate material and EDAX machine background. The elements found for the PMMA-BDK-MR thin films before and after curing (Figs. 16 and 17, respectively) are oxygen (O) and carbon (C). However, hydrogen (H) could not be detected by the EDAX micrographs due to its low atomic number [51]. Figures 18 and 19 show EDAX micrographs of PMMA-BDK-MR/ZnO NPs 1% thin films before and after curing, respectively. In addition to the elements of the reference PMMA-BDK-MR, it contains Zn element as expected. Moreover, the EDAX micrographs show the mapping of each element

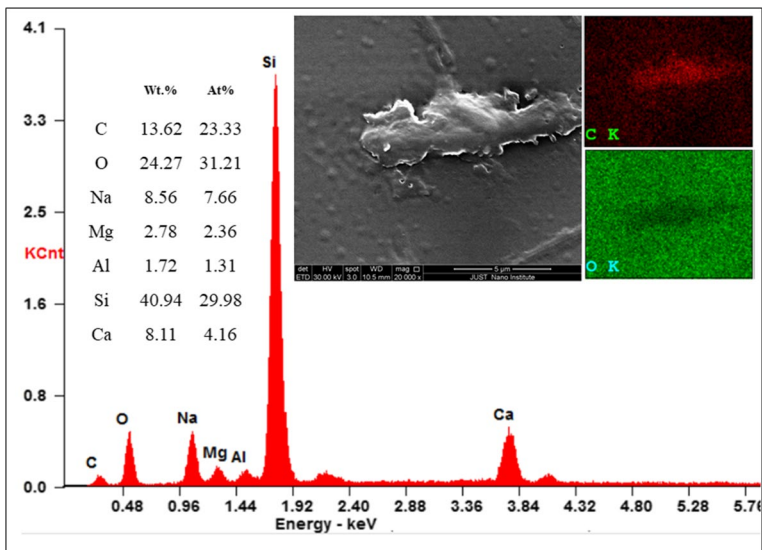


Fig. 16 EDAX micrographs and mapping of undoped PMMA-BDK-MR without curing

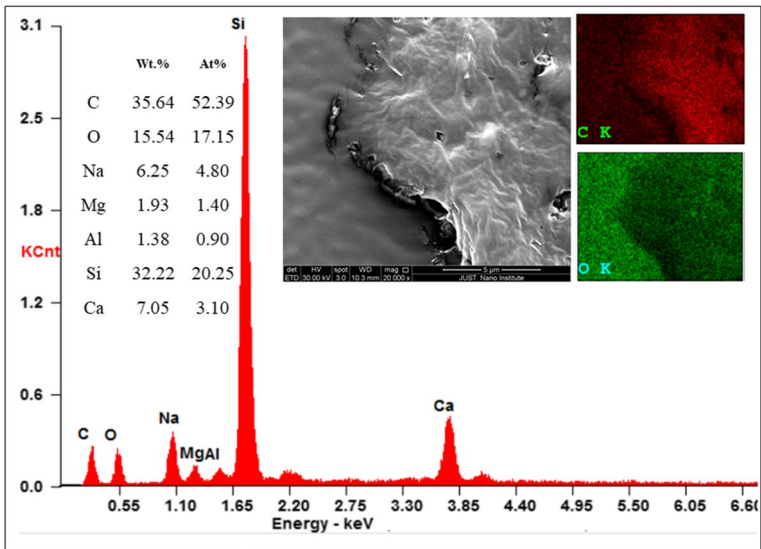


Fig. 17 EDAX micrographs and mapping of undoped PMMA-BDK-MR with curing

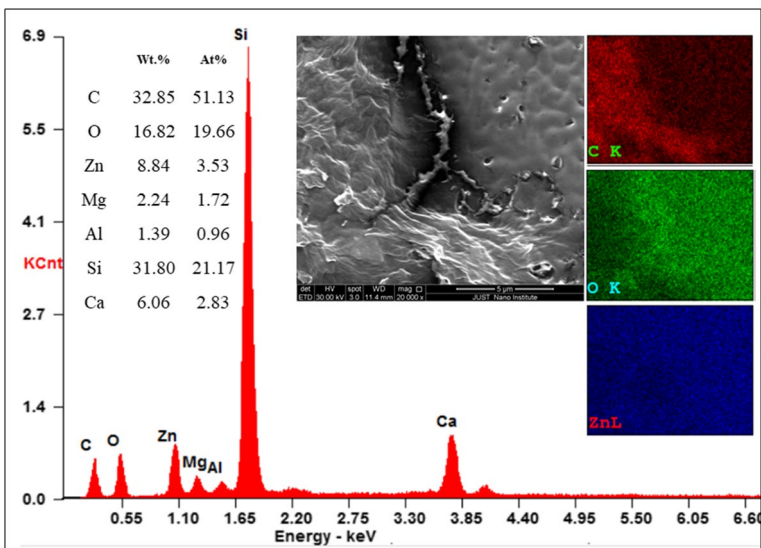


Fig. 18 EDAX micrographs and mapping of PMMA-BDK-MR/ZnO NPs 1% without curing

presented in the microstructure of thin films. We have chosen to show the mapping micrographs of Zn, O and C elements. We found that Zn atoms are distributed uniformly in the structure of thin films. This is crucial as it is very important to control the dispersion homogeneity of the nanoparticles over the entire matrix because this

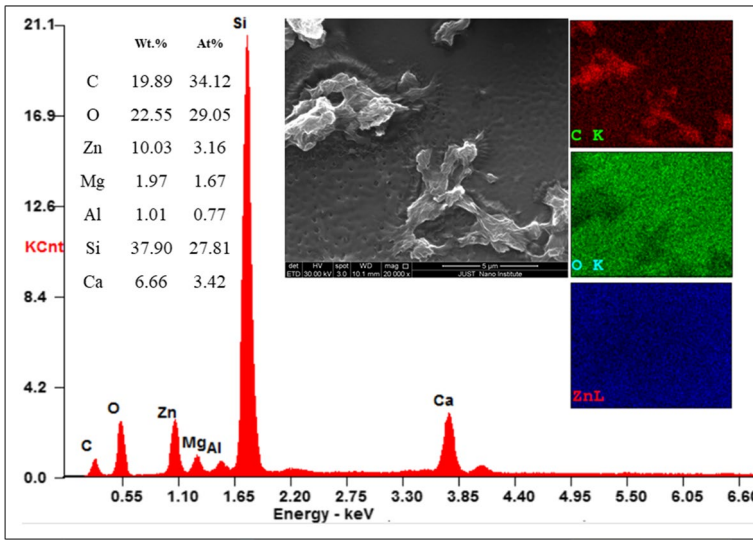


Fig. 19 EDAX micrographs and mapping of PMMA-BDK-MR/ZnO NPs 1% with curing

has a great influence on the optical characteristic and some other functions of the nanohybrid thin films [66].

Thermogravimetric analysis (TGA)

The thermal stability of PMMA-BDK-MR/ZnO NPs thin films for different ZnO NPs concentrations is investigated using thermogravimetric analysis (TGA). The TGA is performed for undoped PMMA-BDK-MR and 1%, 2%, 4% PMMA-BDK-MR/ZnO NPs thin films for temperature range (0–400 °C) as illustrated in Fig. 20. The figure shows the TGA profiles of PMMA-BDK-MR/ZnO NPs thin films. As indicated by the figure, the weight loss of PMMA-BDK-MR/ZnO NPs thin films

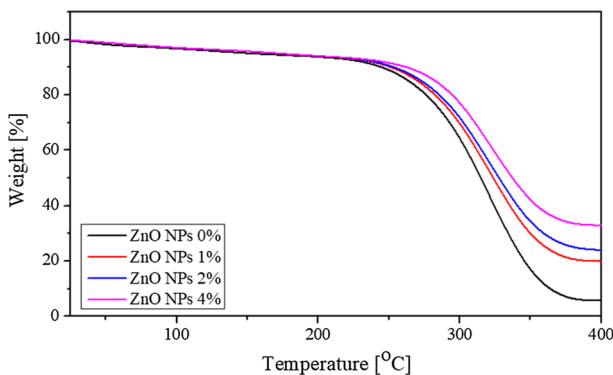


Fig. 20 TGA curves of PMMA-BDK-MR/ZnO NPs thin films with various ZnO NPs concentrations

below 250 °C is about 10% that is, attributed to the physisorbed water and residual organic solvent. As for PMMA-BDK-MR/ZnO NPs nanocomposite, the beginning of the decomposition at 250 °C corresponds to the decomposed temperature of PMMA-BDK-MR covalently attached to ZnO NPs. The weight loss has decreased from 94 to 80% when ZnO NPs with a concentration of 1% are introduced in the polymer matrix. Furthermore, the weight loss has decreased to 76% and 67% as ZnO NPs with a concentration of 2% and 4% are introduced in the polymer matrix, respectively. Our findings are in good agreement with previously published works [67, 68]. The inverse proportionality of the weight loss of nanocomposites with the ZnO NPs concentration indicate that, as the concentration of ZnO NPs introduced in the polymer matrix is increased, the physicochemical bonding density of the polymer is strengthened.

Conclusions

In summary, PMMA-BDK-MR polymers doped by 1%, 2% and 4% of ZnO NPs in the form of thin films were prepared by dip coating technique. The effects of doping the polymer with ZnO NPs on the thin films optical properties, surface morphology have been studied and interpreted. We investigated thermal stability of PMMA-BDK-MR/ZnO NPs thin films using thermogravimetric analysis (TGA). We found that the weight loss has decreased from 94 to 80%, 76% and 67% as ZnO NPs with concentrations of 1%, 2% and 4% are introduced in the polymer matrix, respectively. Owing to their obtained properties, we investigated the possibility of using the doped PMMA-BDK-MR polymer films as optical data storage media or optical and thermal sensors. The optical properties of the resulting thin films were characterized by performing transmittance and reflectance measurements. The absorption coefficient (α), optical band gap energy (E_g), Urbach energy (E_U), dielectric functions (ϵ_1 and ϵ_2) and dielectric loss tangent ($\tan \delta$) have been calculated accordingly. In addition, we investigated the possibility of using such doped polymeric thin films for optical data storage media, WRE cyclic process of transferring the electrochemical bonding from *trans* to *cis* and vice versa. We found that upon illuminating thin films with UV light in the *trans* absorption band, they transform from *trans* to *cis* configuration due to light induced photoisomerization. In addition, a *cis* form could be transversed back to a *trans* form by means of thermal relaxation process. Remarkably, this change in structure *trans* \leftrightarrow *cis* can be utilized for memory WRITE and memory READ applications. We found that PMMA-BDK-MR-1% ZnO NPs thin films cured with 366 nm UV light for 10 undergo *trans* \leftrightarrow *cis* cycles successfully indicating the feasibility and validity of using this thin film as an optical data storage media by means of “on” and “off” states. Finally, we studied the morphology of the thin film surface by SEM, EDAX and mapping. We found that the surfaces of PMMA-BDK-MR and PMMA-BDK-MR/ZnO NPs 1% thin films without curing are both inhomogeneous compared with the corresponding surfaces after curing. The transformation from inhomogeneous surfaces to homogeneous surfaces is attributed to the polymerization of thin films by UV curing.

Acknowledgement The authors would like to acknowledge Jordan University of Science and Technology (JUST) in Jordan for technical and financial support received from the Deanship of Scientific Research (scientific project #20160166).

References

1. Lü N, Lü X, Jin X, Lü C (2007) Preparation and characterization of UV-curable ZnO/polymer nanocomposite films. *Polym Int* 56:138–143
2. Innocenzi P, Esposito M, Maddalena A (2001) Mechanical properties of 3-glycidioxypropyltrimethoxysilane based hybrid organic-inorganic materials. *J Sol-Gel Sci Technol* 20:293–301
3. Lü C, Cui Z, Guan C, Guan J, Yang B, Shen J (2003) Research on preparation, structure and properties of TiO₂/polythiourethane hybrid optical films with high refractive index. *Macromol Mater Eng* 288:717–723
4. Hsu SC, Whang WT, Hung CH, Chiang PC, Hsiao YN (2005) Effect of the polyimide structure and ZnO concentration on the morphology and characteristics of polyimide/ZnO nanohybrid films. *Macromol Chem Phys* 206:291–298
5. Grasset F, Saito N, Li D, Park D, Sakaguchi I, Ohashi N et al (2003) Surface modification of zinc oxide nanoparticles by aminopropyltriethoxysilane. *J Alloy Compd* 360:298–311
6. Novak BM (1993) Hybrid nanocomposite materials—between inorganic glasses and organic polymers. *Adv Mater* 5:422–433
7. Guo B, Liu Z, Hong L, Jiang H (2005) Sol gel derived photocatalytic porous TiO₂ thin films. *Surf Coat Technol* 198:24–29
8. Nimittrakoolchai O-U, Supothina S (2008) Deposition of organic-based superhydrophobic films for anti-adhesion and self-cleaning applications. *J Eur Ceram Soc* 28:947–952
9. Yamashita H, Nishio S, Katayama I, Nishiyama N, Fujii H (2006) Photo-induced super-hydrophilic property and photocatalysis on transparent Ti-containing mesoporous silica thin films. *Catal Today* 111:254–258
10. Messori M, Toselli M, Pilati F, Fabbri E, Fabbri P, Busoli S et al (2003) Flame retarding poly (methyl methacrylate) with nanostructured organic-inorganic hybrids coatings. *Polymer* 44:4463–4470
11. Zhu LJ, Wang JJ, Guo L, Shen J (2011) Study on the preparation and properties of the PVA/SiO₂ hybrid coating on BOPP film via sol-gel process. In: *Advanced materials research*, pp 1956–1959
12. Ge J, Zeng X, Tao X, Li X, Shen Z, Yun J et al (2010) Preparation and characterization of PS-PMMA/ZnO nanocomposite films with novel properties of high transparency and UV-shielding capacity. *J Appl Polym Sci* 118:1507–1512
13. Khrenov V, Klapper M, Koch M, Müllen K (2005) Surface functionalized ZnO particles designed for the use in transparent nanocomposites. *Macromol Chem Phys* 206:95–101
14. Levine KL, Iroh JO, Kosel PB (2004) Synthesis and properties of the nanocomposite of zinc oxide and poly (amic acid). *Appl Surf Sci* 230:24–33
15. Hung C-H, Whang W-T (2005) Effect of surface stabilization of nanoparticles on luminescent characteristics in ZnO/poly (hydroxyethyl methacrylate) nanohybrid films. *J Mater Chem* 15:267–274
16. Abdullah M, Morimoto T, Okuyama K (2003) Generating Blue and Red Luminescence from ZnO/Poly (ethylene glycol) nanocomposites prepared using an in-situ method. *Adv Func Mater* 13:800–804
17. Xiong H-M, Zhao X, Chen J-S (2001) New polymer-inorganic nanocomposites: PEO-ZnO and PEO-ZnO-LiClO₄ films. *J Phys Chem B* 105:10169–10174
18. Zheng J, Siegel RW, Toney CG (2003) Polymer crystalline structure and morphology changes in nylon-6/ZnO nanocomposites. *J Polym Sci Part B Polym Phys* 41:1033–1050
19. Liu B, Wang M, He Y, Wang X (2006) Duplication of photoinduced azo polymer surface-relief gratings through a soft lithographic approach. *Langmuir* 22:7405–7410
20. Kawata S, Kawata Y (2000) Three-dimensional optical data storage using photochromic materials. *Chem Rev* 100:1777–1788
21. Natansohn A, Rochon P (1999) Photoinduced motions in azobenzene-based amorphous polymers: possible photonic devices. *Adv Mater* 11:1387–1391

22. Yager KG, Barrett CJ (2006) Photomechanical surface patterning in azo-polymer materials. *Macromolecules* 39:9320–9326
23. Czaplicki R, Krupka O, Essaidi Z, El-Ghayoury A, Kajzar F, Grote J et al (2007) Grating inscription in picosecond regime in thin films of functionalized DNA. *Opt Express* 15:15268–15273
24. Schab-Balcerzak E, Flakus H, Jarczyk-Jedryka A, Konieczkowska J, Siwy M, Bijak K et al (2015) Photochromic supramolecular azopolyimides based on hydrogen bonds. *Opt Mater* 47:501–511
25. Derkowska-Zielinska B, Skowronski L, Kozłowski T, Smokal V, Kysil A, Biitseva A et al (2015) Influence of peripheral substituents on the optical properties of heterocyclic azo dyes. *Opt Mater* 49:325–329
26. Stoilova A, Georgiev A, Nedelchev L, Nazarova D, Dimov D (2019) Structure-property relationship and photoinduced birefringence of the azo and azo-azomethine dyes thin films in PMMA matrix. *Opt Mater* 87:16–23
27. Kozanecka-Szmigiel A, Switkowski K, Schab-Balcerzak E, Szmigiel D (2015) Photoinduced birefringence of azobenzene polymer at blue excitation wavelengths. *Appl Phys B* 119:227–231
28. Merino E, Ribagorda M (2012) Control over molecular motion using the cis–trans photoisomerization of the azo group. *Beilstein J Org Chem* 8:1071–1090
29. Yager KG, Barrett CJ (2009) Azobenzene polymers for photonic applications. *Smart Light Responsive Mater* 1:1–46
30. Derkowska-Zielinska B, Skowronski L, Biitseva A, Grabowski A, Naparty M, Smokal V et al (2017) Optical characterization of heterocyclic azo dyes containing polymers thin films. *Appl Surf Sci* 421:361–366
31. Combellas C, Kajzar F, Mathey G, Petit MA, Thiébault A (2000) Zwitterionic polymers for non-linear optics. *Chem Phys* 252:165–177
32. Large M, Kajzar F, Raimond P (1998) Modulation of second harmonic generation in photochromic materials by the application of electric fields and low intensity light. *Appl Phys Lett* 73:3635–3637
33. Luo Y, She W, Wu S, Zeng F, Yao S (2005) Improvement of all-optical switching effect based on azobenzene-containing polymer films. *Appl Phys B* 80:77–80
34. Mohajerani E, Heydari E (2007) Trans-cis-trans photoisomerization as an all-optical switching in azo-dye-doped polymer waveguide. In: *Light-emitting diode materials and devices II*, p 682818
35. Yan D, Yan-Hua L, Pei W, Yong-Hua L, Hai M, Qi-Jing Z (2007) All-optical switching based on azo polymer material. *Chin Phys Lett* 24:2849
36. Henari FZ, Cassidy S (2012) Non-linear optical properties and all optical switching of Congo red in solution. *Optik* 123:711–714
37. Zhao J, Dong F, Qu H, Ye P, Fu X, Qiu L et al (1995) Dynamic studies on laser-induced gratings in azobenzene-doped polymer film. *Appl Phys B* 61:377–384
38. Dumont M (1993) Photopolymers and applications in holography, optical data storage, optical sensors, and interconnects. In: *Proc. SPIE*, p 2
39. Lee GJ, Kim D, Lee M (1995) Photophysical properties and photoisomerization processes of Methyl Red embedded in rigid polymer. *Appl Opt* 34:138–143
40. Shi Y, Steier WH, Yu L, Chen M, Dalton LR (1991) Large stable photoinduced refractive index change in a nonlinear optical polyester polymer with disperse red side groups. *Appl Phys Lett* 58:1131–1133
41. Sekkat Z, Morichere D, Dumont M, Loucif-Saïbi R, Delaire J (1992) Photoisomerization of azobenzene derivatives in polymeric thin films. *J Appl Phys* 71:1543–1545
42. Coelho PJ, Sousa CM, Castro MCR, Fonseca AMC, Raposo MMM (2013) Fast thermal cis–trans isomerization of heterocyclic azo dyes in PMMA polymers. *Opt Mater* 35:1167–1172
43. Feringa BL, Jager WF, de Lange B (1993) Organic materials for reversible optical data storage. *Tetrahedron* 49:8267–8310
44. Ahmad A, Omari, A (2015) The UV and laser aging for PMMA/BDK/Azo-dye polymer blend cured by UV light beams. In: *IOP conference series: materials science and engineering*, p 012024
45. Blasco E, Piñol M, Berges C, Sánchez-Somolinos C, Oriol L (2019) Smart polymers for optical data storage. In: Aguilar MR, Roman JS (eds) *Smart polymers and their applications*. Elsevier, pp 567–606
46. Al Attar HA, Taqatqa O (2003) A new highly photorefractive polymer composite for optical data storage application. *J Opt A Pure Appl Opt* 5:S487

47. Webb R, Langford S, Dickinson J, Lippert T (1998) Sensitization of PMMA to laser ablation at 308 nm. *Appl Surf Sci* 127:815–820
48. Yang Z, Ji S, Gao W, Zhang C, Ren L, Tjiu WW et al (2013) Magnetic nanomaterial derived from graphene oxide/layered double hydroxide hybrid for efficient removal of methyl orange from aqueous solution. *J Colloid Interface Sci* 408:25–32
49. Ginsburg JC (2004) The right to claim authorship in US copyright and trademarks law. *Houst Law Rev* 41:263
50. Duarte F, Maldonado-Hódar F, Pérez-Cadenas A, Madeira LM (2009) Fenton-like degradation of azo-dye Orange II catalyzed by transition metals on carbon aerogels. *Appl Catal B* 85:139–147
51. Ahmad A, Alsaad A, Al-Bataineh Q, Al-Naafa M (2018) Optical and structural investigations of dip-synthesized boron-doped ZnO-seeded platforms for ZnO nanostructures. *Appl Phys A* 124:458
52. Ahmad A, Alsaad A, Al-Bataineh Q, Bani-Salameh A, Al-Khateeb H, Al-Naafa M (2017) Optical and structural characterization of dip synthesized Al-B Co-doped ZnO seeded platforms for ZnO nanostructures. *Jordan J Phys* 10:2017
53. Jin M, Yang QX, Lu R, Pan LY, Xue PC, Zhao Y (2003) Synthesis and photo-induced birefringence of pyrazoline substituted azo-dyes in PMMA films. *Opt Mater* 24:445–452
54. Al-Bataineh QM, Alsaad A, Ahmad A, Al-Sawalmih A (2019) Structural, electronic and optical characterization of ZnO thin film-seeded platforms for ZnO nanostructures: sol-gel method versus ab initio calculations. *J Electron Mater* 48:5028–5038
55. Wang G, Hou L, Gan F (1999) Optical storage properties of novel azo dye-in-polymer (PMMA) thin films. *Phys Status Solidi (a)* 174:269–275
56. Wu P-C, Hou C-T, Hsiao Y-C, Lee W (2014) Influence of methyl red as a dopant on the electrical properties and device performance of liquid crystals. *Opt Express* 22:31347–31355
57. Urbach F (1953) The long-wavelength edge of photographic sensitivity and of the electronic absorption of solids. *Phys Rev* 92:1324
58. El-Hagary M, Emam-Ismael M, Shaaban E, El-TaHER A (2012) Effect of γ -irradiation exposure on optical properties of chalcogenide glasses Se70S30-xSbx thin films. *Radiat Phys Chem* 81:1572–1577
59. Tauc J (2012) *Amorphous and liquid semiconductors*. Springer, Berlin
60. Bhattacharyya D, Chaudhuri S, Pal A (1992) Bandgap and optical transitions in thin films from reflectance measurements. *Vacuum* 43:313–316
61. Shahane G, More B, Rotti C, Deshmukh L (1997) Studies on chemically deposited CdS_{1-x}Sex mixed thin films. *Mater Chem Phys* 47:263–267
62. Hassanien AS, Akl AA (2015) Influence of composition on optical and dispersion parameters of thermally evaporated non-crystalline Cd₅₀S_{50-x}Sex thin films. *J Alloy Compd* 648:280–290
63. Jin ZC, Hamberg I, Granqvist C (1988) Optical properties of sputter-deposited ZnO: Al thin films. *J Appl Phys* 64:5117–5131
64. Chamroukhi H, Hamed ZB, Telfah A, Bassou M, Zeinert A, Hergenröder R et al (2018) Optical and structural properties enhancement of hybrid nanocomposites thin films based on polyaniline doped with Zinc Oxide embedded in bimodal mesoporous silica (ZnO@ SiOX) nanoparticles. *Opt Mater* 84:703–713
65. Cao M-S, Song W-L, Hou Z-L, Wen B, Yuan J (2010) The effects of temperature and frequency on the dielectric properties, electromagnetic interference shielding and microwave-absorption of short carbon fiber/silica composites. *Carbon* 48:788–796
66. Pesika NS, Hu Z, Stebe KJ, Searson PC (2002) Quenching of growth of ZnO nanoparticles by adsorption of octanethiol. *J Phys Chem B* 106:6985–6990
67. Rawat A, Soni U, Malik RS, Pandey SC (2018) Facile synthesis of UV blocking nano-sized Zinc Oxide and Polymethyl-methacrylate polymer nanocomposite coating material. *Nano Struct Nano Objects* 16:371–380
68. Quadri TW, Olasunkanmi LO, Fayemi OE, Solomon MM, Ebenso EE (2017) Zinc oxide nanocomposites of selected polymers: synthesis, characterization, and corrosion inhibition studies on mild steel in HCl solution. *ACS Omega* 2:8421–8437